JOURNAL OF SPACECRAFT AND ROCKETS
Vol. 34, No. 2, March–April 1997

Spacecraft Orbits Around Asteroids for Global Mapping

Masayoshi Utashima*
National Space Development Agency, Tsukuba-shi 305, Japan

A study is presented on spacecraft orbits around asteroids, the purpose of which is to observe asteroids globally with high resolution. Objects of the study are asteroids smaller than 100 km in size with orbital radii between 1.5 and 3 AU. If the radiation pressure is the only perturbation, a frozen orbit whose Keplerian mean elements do not change exists. There are two kinds of frozen orbits: one is the orbit in the orbital plane of the asteroid, which is not adequate for high-resolution observation, and the other is the solar plane-of-sky orbit, which is adequate for the asteroids whose radii are below 2 or 3 km. The polar orbit, which is suitable for the global observation and has the merit that effects of the oblateness disappear, was also studied. Basically, the maintenance of the polar orbit requires only making the eccentricity zero. The maintenance was investigated by numerical integrations for the averaged orbital elements considering the solar radiation pressure and the oblateness. When the ratio of the characteristic angular velocity due to the radiation pressure and the one due to the oblateness multiplied by the eccentricity limit for the maintenance is smaller than about 1, the maintenance is not necessary.

Nomenclature

a = mean semimajor axis of the spacecraft orbit around the asteroid
B = mass-to-cross section ratio of the spacecraft, m/S
C_p = characteristic angular velocity due to the radiation pressure
C_R = reflection coefficient of the spacecraft
C_s = characteristic angular velocity due to the oblateness of the asteroid
e_f = eccentricity of the frozen orbit
e_{limit} = eccentricity limit of the spacecraft polar orbit around the asteroid
$\boldsymbol{F}_R$ = acceleration vector due to the radiation pressure acting on the spacecraft
G = universal gravitational constant, 6.672×10^{-11} m^3/(kg · s)^2
G_1 = solar constant, $P_E R_E^2$, 1.0218×10^{17} N
I = inclination of the spacecraft orbit around the asteroid in the equatorial coordinate system of the asteroid
i = inclination of the spacecraft orbit around the asteroid in the orbital plane coordinate system of the asteroid
J = angle between the equator and the orbital plane of the asteroid
J_2 = second-order zonal term coefficient of the gravitational potential of the asteroid
J_4 = fourth-order zonal term coefficient of the gravitational potential of the asteroid
m = mass of the spacecraft
N = right ascension of the ascending node of the spacecraft orbit around the asteroid in the equatorial coordinate system of the asteroid
n = mean motion of the spacecraft orbit
P = radiation pressure at the asteroid, G_1/R^2
P_E = radiation pressure at the Earth, 4.566×10^{-6} N/m^2
R = distance between the sun and the asteroid
R_E = radius of the Earth orbit, 1.496×10^{11} m
S = cross-sectional area of the spacecraft
T = period of the spacecraft orbit around the asteroid
$\boldsymbol{u}_g$ = unit vector with the antisolar direction from the center of the asteroid
W = argument of periapsis of the spacecraft orbit around the asteroid in the equatorial coordinate system of the asteroid
α = maximum radius of the asteroid
$\hat{\beta}$ = middle radius of the asteroid / α
$\hat{\gamma}$ = minimum radius of the asteroid / α
ΔV_N = velocity increment required for the cancellation of the eccentricity change due to the radiation pressure
ΔV_p = velocity increment required for the cancellation of the orbital plane change due to the oblateness
ΔV_ω = velocity increment required for the cancellation of the periapsis direction change due to the oblateness
η = second component of the eccentricity vector of the spacecraft orbit around the asteroid
θ = antisolar direction angle measured from the vernal equinox of the asteroid
μ_s = solar gravitational constant, 1.3272×10^{20} m^3/s^2
ξ = first component of the eccentricity vector of the spacecraft orbit around the asteroid
ρ = density of the asteroid
Ω = right ascension of the ascending node of the spacecraft orbit around the asteroid in the orbital plane coordinate system of the asteroid
ω = argument of periapsis of the spacecraft orbit around the asteroid in the orbital plane coordinate system of the asteroid

Introduction

ASTEROIDS exploration, as well as planetary exploration, such as for Mars and Jupiter, has recently attracted considerable attention. It is expected that asteroid exploration will bring us valuable information about the formation of the solar system. The first asteroidal orbiting mission, Near-Earth Asteroid Rendezvous (NEAR), spacecraft was launched to 433 Eros in February of 1996 (Ref. 1). MUSES-C spacecraft will be launched to 4660 Nereus in 2002 as the first sample return mission except for the moon.[2]

This paper presents the results of a study of spacecraft orbits around asteroids, the primary purpose of which is to observe asteroids globally with high resolution. All of the asteroids, whose sizes (maximum radii) are below 100 km and whose orbital radii are between 1.5 and 3 AU, are objects for this study. Orbits of asteroids are assumed to be circular for simplicity. The altitude of the spacecraft orbit is limited to be greater than about three times the radius of the asteroid to avoid the significant instability due to the irregular shape of asteroids.

Received July 1, 1996; revision received Dec. 22, 1996; accepted for publication Jan. 3, 1997.

*Associate Senior Engineer, Office of Research and Development, Sengen 2-1-1. Member AIAA.

Outline of Acceleration Field Around Asteroid

Though asteroids are small, they can have satellites by their own gravitation. The sizes of the sphere of influence[3] for 433 Eros and 4660 Nereus are for Eros about 500 km (25 times the maximum radius) and for Nereus about 14 km (14 times the maximum radius). Both distances between the sun and the asteroids are assumed to be 1.5 AU.

Sources of the primary perturbations on the orbit around an asteroid are 1) solar radiation pressure, 2) irregular shape of the asteroid, and 3) solar tidal force. The second source is dominant inside the area of 2–3 times of the asteroid's radius. Source 3 is dominant where far from the asteroid. Because sources 1 and 2 are dominant in the region of study, source 3 is ignored.[4]

Effects from the irregular shape of the asteroid can be avoided by adopting a retrograde orbit near the equator.[5] Those orbits, however, may not be suitable for the global mapping of the asteroid.

Conditions for Study

The objects of this study are asteroids whose maximum radii are smaller than 100 km and whose orbital sizes are between 1.5 and 3 AU. The mean density of asteroids is approximated to be 3.5 g/cm^3. Orbits of asteroids are assumed to be circular for simplicity.

The spacecraft is assumed to have a mass-to-cross section ratio of 30 kg/m^2. NEAR spacecraft has a value of about 41 kg/m^2. The reflection coefficient C_R of the spacecraft is approximated to be 1.5. C_R of 1.0 means perfect absorption, and C_R of 2.0 means perfect reflection. An imager onboard is assumed to have 1-m resolution from a 100-km distance.

Variation Rates of Mean Orbital Elements

The variation rates of the mean orbital elements due to the solar radiation pressure and the irregular shape of the asteroid are described in this section.

Variation Rates due to Solar Radiation Pressure

The acceleration vector $\boldsymbol{F}_R$ due to the solar radiation pressure acting on the spacecraft is given by

$$\boldsymbol{F}_R = F_R \boldsymbol{u}_g \tag{1}$$

$$F_R = P(S/m)C_R = P(C_R/B)$$

The variation rates of the mean orbital elements due to the radiation pressure are shown next. They can be obtained from the mean disturbing function, which is derived by averaging the disturbing function that introduces the acceleration of Eq. (1) (Ref. 6):

$$\frac{\mathrm{d}a}{\mathrm{d}t} = 0 \qquad \frac{\mathrm{d}e}{\mathrm{d}t} = -\frac{3}{2}\frac{\sqrt{1-e^2}}{na}F_R \left\{ \begin{array}{l} \sin\omega\cos(\Omega-\theta) \\ +\cos i\cos\omega\sin(\Omega-\theta) \end{array} \right\}$$

$$\frac{\mathrm{d}i}{\mathrm{d}t} = -\frac{3}{2}\frac{e}{na\sqrt{1-e^2}}F_R \sin i\cos\omega\sin(\Omega-\theta) \tag{2}$$

$$\frac{\mathrm{d}\Omega}{\mathrm{d}t} = -\frac{3}{2}\frac{e}{na\sqrt{1-e^2}}F_R \sin\omega\sin(\Omega-\theta)$$

$$\frac{\mathrm{d}\omega}{\mathrm{d}t} = -\frac{3}{2}\frac{\sqrt{1-e^2}}{nae}F_R \left\{ \begin{array}{l} \cos\omega\cos(\Omega-\theta) \\ -\cos i\sin\omega\sin(\Omega-\theta) \end{array} \right\} - \cos i\frac{\mathrm{d}\Omega}{\mathrm{d}t}$$

Equation (2) is based on the coordinate system consisting of the asteroid's orbital plane as the reference plane and the vernal equinox of the asteroid as the reference direction (Fig. 1). Hereafter, we call it the orbital plane coordinate system. Here, we define the characteristic angular velocity due to the radiation pressure C_p by

$$C_p = \tfrac{3}{2}(F_R/na) \tag{3}$$

Variation Rates due to Irregular Shape

According to Ref. 5, secular perturbations of the orbit whose semimajor axis is larger than about three times the radius of the asteroid due to the irregular shape can be evaluated with good accuracy by Kozai's theory considering J_2 and J_4 terms.

Table 1 Characteristics of three asteroids

Name	Ida	Eros	Gaspra
Maximum radius α, km	26.5	20.0	9.5
Middle radius/α ($\hat{\beta}$)	0.43	0.35	0.63
Minimum radius/α ($\hat{\gamma}$)	0.34	0.35	0.63
J_2	0.096	0.088	0.073
J_4	−0.0267	−0.0248	−0.0152
Semimajor axis, AU	2.86	1.46	2.21
Eccentricity	0.042	0.223	0.174

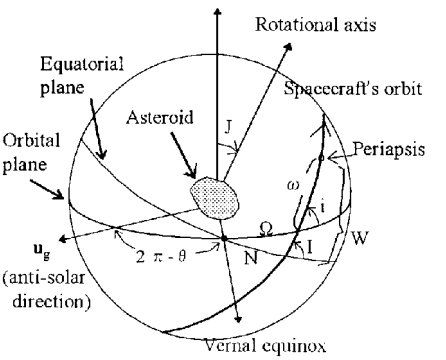

Fig. 1 Orbital plane and equatorial coordinate systems of asteroid.

Table 1 shows the shapes and orbits of three asteroids: 243 Ida, 433 Eros, and 951 Gaspra. In this paper, only α is changed, and $\hat{\beta} = 0.5$ and $\hat{\gamma} = 0.35$ are fixed. J_2 is approximated by Eq. (4) for the triaxial ellipsoid with the radius ratio of $1{:}\hat{\beta}{:}\hat{\gamma}$ (Ref. 5):

$$J_2 = \tfrac{1}{10}(1 + \hat{\beta}^2 - 2\hat{\gamma}^2) \tag{4}$$

For $\hat{\beta} = 0.5$ and $\hat{\gamma} = 0.35$, $J_2 = 0.1005$ is obtained. Effects by J_4 terms are less than 3% of those of J_2 terms in this asteroid model for $a/\alpha > 3$. Therefore, only J_2 terms are used hereafter.

The secular rates of both the right ascension of ascending node N and the argument of periapsis W by J_2 terms are described by

$$\frac{\mathrm{d}N}{\mathrm{d}t} = -\frac{3}{2}\frac{\alpha^2 J_2}{a^2(1-e^2)^2}n\cos I$$

$$\frac{\mathrm{d}W}{\mathrm{d}t} = \frac{3}{2}\frac{\alpha^2 J_2}{a^2(1-e^2)^2}n\left(2 - \frac{5}{2}\sin^2 I\right) \tag{5}$$

Here, we define the characteristic angular velocity due to J_2 terms C_s by

$$C_s = \tfrac{3}{2}\left(\alpha^2 J_2 / a^2\right)n \tag{6}$$

Applicability of Frozen Orbit

The solar radiation pressure is the principal perturbation for orbits whose sizes are several times the asteroid's radius. The frozen orbits whose Keplerian mean elements do not change exist under the condition that the radiation pressure is the only perturbation.[4] The feasible region for the frozen orbits is studied from the viewpoint of observation with high resolution in the plane consisting of the maximum radius of asteroids and the semimajor axis of the spacecraft orbit.

Necessary Conditions for Frozen Orbits

The averaged Keplerian elements are used. This approach neglects a dynamical effect of the radiation pressure that causes an offset of the orbital plane from the center of the asteroid. Because the author has not evaluated it quantitatively as yet, a constraint that the offset should be smaller than $\frac{1}{10}$ of the maximum radius of the asteroid is used here tentatively. Hereafter, the validity of this $\frac{1}{10}$ should be checked by numerical simulations. This constraint is expressed by

$$\frac{a}{\alpha} \le \left(\frac{2\pi G\rho\hat{\beta}\hat{\gamma}}{15G_1 C_R}\right)^{\frac{1}{3}} B^{\frac{1}{3}} R^{\frac{2}{3}} \alpha^{\frac{1}{3}} \tag{7}$$

Eccentricity of Frozen Orbit

There are two kinds of frozen orbits: one in which the orbital plane corresponds with the orbital plane of the asteroid, the other's orbital plane is perpendicular to the solar direction. The former is called the frozen orbit in the orbital plane; the latter is called the solar plane-of-sky frozen orbit. For both orbits a/α is obtained by[4]

$$\frac{a}{\alpha} = \frac{16\pi G\mu_s \rho\hat{\beta}\hat{\gamma}}{27G_1^2C_R^2} RB^2\alpha^2\Lambda^2 \tag{8}$$

Λ in Eq. (8) is given by the eccentricity of the frozen orbit for the orbit in the orbital plane and the solar plane-of-sky orbit, respectively, as[4]

$$\Lambda = \begin{cases} \dfrac{e_f}{\sqrt{1-e_f^2}} & \text{(orbit in the orbital plane)} \\ \dfrac{\sqrt{1-e_f^2}}{e_f} & \text{(solar plane-of-sky orbit)} \end{cases} \tag{9}$$

Region Where Radiation Pressure Is Dominant

From the condition that the characteristic angular velocity for the radiation pressure is larger than k times of that for the oblateness,

$$\frac{a}{\alpha} \geq \left(\frac{4k\pi G\rho J_2\hat{\beta}\hat{\gamma}}{3G_1C_R}\right)^{\frac{1}{4}} B^{\frac{1}{4}}R^{\frac{1}{2}}\alpha^{\frac{1}{4}} \tag{10}$$

is obtained. J_2 is fixed to 0.1, and $k = 10$ is used in this study.

Constraint of Altitude

The altitude of the spacecraft orbit is limited to $H_{\max}$ by the following in order to secure the resolution at observation:

$$a/\alpha \leq 1 + (H_{\max}/\alpha) \tag{11}$$

Feasible Region for Frozen Orbits

Figures 2 and 3 show the feasible regions (vertical hatching) for the frozen orbit in the orbital plane and the solar plane-of-sky orbit, respectively. Figure 2 shows that the feasible region of α is very small and about 40–50 km. The limiting factor for the smaller α is the eccentricity of 0.3, and the one for the larger α is the altitude constraint of 1000 km. The expected resolution is about 7–10 m. It turned out that the frozen orbits in the orbital plane are not enough for the high-resolution observation.

Though no common area to Eqs. (7) and (10) with $k = 10$ exists in Fig. 3, we consider the region around the hatched area to be feasible because the constraint by Eq. (7) might be relaxed. Asteroids whose maximum radii are smaller than about 3 km are feasible. The limiting factor is the eccentricity of 0.3. Because the altitude for the feasible region is low, resolution less than 1 m is expected.

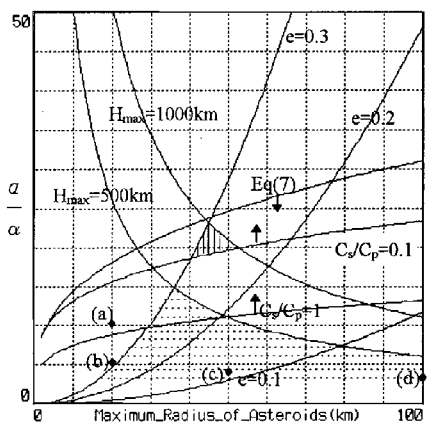

Fig. 2 Feasible region for the frozen orbit in the orbital plane: R = 2 AU and B = 30 kg/m^2.

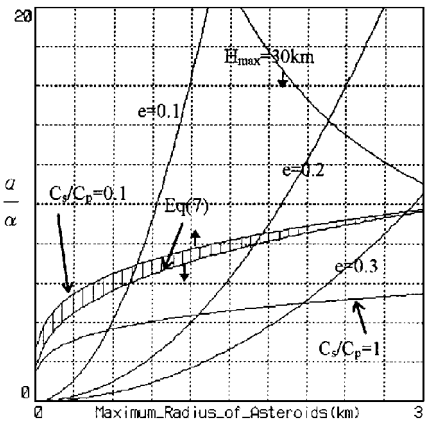

Fig. 3 Feasible region for the solar plane-of-sky orbit: R = 2 AU and B = 30 kg/m^2.

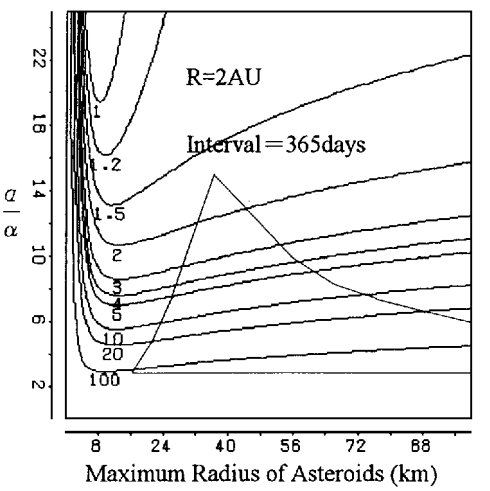

Fig. 4 Maintenance ΔV for the frozen orbit in the orbital plane: R = 2 AU and B = 30 kg/m^2.

Maintenance of Frozen Orbits in the Orbital Plane

Because the frozen orbits in the orbital plane have large altitudes, the maintenance of the lower frozen orbits in the orbital plane by maneuvers is studied. The desired region is shown in Fig. 2 by horizontal dotted lines. In this region, rotations of both the orbital plane and the periapsis by the oblateness of the asteroid should be canceled by maneuvers.

The velocity increment for canceling the rotation of the orbital plane during Δt is evaluated by

$$\Delta V_p = \frac{3}{4}\frac{aJ_2n^2}{(a/\alpha)^2(1-e^2)^2}|\sin 2J|\Delta t \qquad n^2 = \frac{4}{3}\pi\rho\frac{\hat{\beta}\hat{\gamma}G}{(a/\alpha)^3} \tag{12}$$

The velocity increment for canceling the rotation of the periapsis during Δt is evaluated by

$$\Delta V_\omega = (na/2)e|\dot{W} + \dot{N}\cos J - \dot{\theta}|\Delta t \qquad \text{(for } i = 0\text{)}$$

$$\Delta V_\omega = (na/2)e|\dot{W} - \dot{N}\cos J + \dot{\theta}|\Delta t \qquad \text{(for } i = \pi\text{)} \tag{13}$$

$$\dot{\theta} = \sqrt{\mu_S/R^3}$$

Thus, the ΔV required for the maintenance is the sum of $\Delta V_p + \Delta V_\omega$ and depends on J. It is said that J is widely distributed because of the collision history of the asteroids. Therefore, the maximum ΔV for various J is used for the evaluation. Figure 4 shows the maximum ΔV for the inclination of 0 deg. The region enclosed by a polygon is the one shown by the horizontal dotted lines in Fig. 2. About 1.7–100 m/s is required for 365 days in this region.

Though ΔV of 100 m/s for 365 days is not a large value, this strategy should be replaced by the polar orbit strategy mentioned in the next section if no special requirements exist.

Polar Orbits Around Asteroids

In this section, we introduce polar orbits around asteroids. Polar orbits have an advantage that the rotation of the asteroid can be utilized for global mapping. The orbital plane of the polar orbit is not affected by the oblateness [see Eq.(5)], and the radiation pressure does not affect orbital planes if the eccentricity is controlled to be zero [see Eq.(2)]. Because the eccentricity is affected by the radiation pressure, it must be maintained near zero by maneuvers. If the fuel cost for these maneuvers is small enough, this strategy is promising.

ΔV for keeping the eccentricity zero is evaluated. Because the eccentricity of near zero is treated, the eccentricity vector defined by Eq. (14) is used:

$$\xi = e\cos\omega \qquad \eta = e\sin\omega \tag{14}$$

The variation rate of the eccentricity at $e = 0$ is evaluated by Eq. (15) using Eqs. (2) and (14):

$$|\dot{e}| = \tfrac{3}{2}(F_R/na)\sqrt{\cos^2(\Omega-\theta) + \cos^2 i \sin^2(\Omega-\theta)} \le \tfrac{3}{2}(F_R/na) \tag{15}$$

Therefore, the required ΔV for the interval of Δt is expressed by

$$\Delta V_N = (na/2)|\dot{e}|\Delta t \le \tfrac{3}{4}F_R\Delta t = \tfrac{3}{4}P(S/m)\Delta t \tag{16}$$

For $\Delta t = 365$ days, $m/S = 30$ kg/m^2 and $R = 2$ AU; $\Delta V_N = 0.9$ m/s is obtained.

This ΔV_N is constant for all of the region in Fig. 4 and is smaller than any value in the polygon of Fig. 4. The advantages of the polar orbit are summarized as follows.

1) The maintenance fuel is significantly small.

2) The rotation of the asteroid can be utilized for mapping.

3) It can be applied to any size of asteroids.

4) Autonomous keeping of the eccentricity may be easy, because the detection of the eccentricity is not difficult by using altimeters.

For the polar orbit to be applied, the rotational motion of the asteroid must be the regular one around the principal axis. The timescale in which the irregular rotation of the asteroid is damped to the simple one is large for asteroids whose radii are small and whose rotational periods are large. For an asteroid with the radius of 1 km and the rotational period of 8 h, the damping timescale is thought to be about 100×10^6 years.[7] Therefore, asteroids whose radii are larger than 10 km can be assumed to be simple rotators.

Simulation of Polar Orbits

By the numerical integration of the mean orbital elements considering the radiation pressure and the oblateness, variations of the eccentricity vector and the orbital plane were studied. Asteroids whose maximum radii are 10–100 km are objects for the simulation. The orbital plane coordinate system is used in the numerical integration.

The variation rates of the mean orbital elements due to the radiation pressure are rewritten using the eccentricity vector as

$$\begin{aligned}
\frac{\mathrm{d}\xi}{\mathrm{d}t} &= -\frac{3}{2}\frac{F_R}{na}\sqrt{1-e^2}\cos i\sin(\Omega-\theta) \\
&\quad -\frac{3}{2}\frac{F_R}{na\sqrt{1-e^2}}\eta^2\cos i\sin(\Omega-\theta) \\
\frac{\mathrm{d}\eta}{\mathrm{d}t} &= -\frac{3}{2}\frac{F_R}{na}\sqrt{1-e^2}\cos(\Omega-\theta) \\
&\quad +\frac{3}{2}\frac{F_R}{na\sqrt{1-e^2}}\xi\eta\cos i\sin(\Omega-\theta) \\
\frac{\mathrm{d}i}{\mathrm{d}t} &= -\frac{3}{2}\frac{F_R}{na\sqrt{1-e^2}}\xi\sin i\sin(\Omega-\theta) \\
\frac{\mathrm{d}\Omega}{\mathrm{d}t} &= -\frac{3}{2}\frac{F_R}{na\sqrt{1-e^2}}\eta\sin(\Omega-\theta)
\end{aligned} \tag{17}$$

Changes of the mean orbital elements due to the oblateness appear in N and W in the equatorial coordinate system of the asteroid [see Eq. (5)]. The eccentricity e and the inclination I do not change by the oblateness. The variation rates of N and W are converted, as shown subsequently, to rates in the orbital plane coordinate system.

From the cosine law (see Fig. 1),

$$\cos i = \cos J\cos I + \sin J\sin I\cos N \tag{18}$$

is derived. By differentiating Eq. (18) and utilizing the sine law,

$$\sin i\sin\Omega = \sin N\sin I \tag{19}$$

the next equation is obtained:

$$\frac{\mathrm{d}i}{\mathrm{d}t} = \sin J\sin\Omega\frac{\mathrm{d}N}{\mathrm{d}t} \tag{20}$$

and $\cos I$ in $\mathrm{d}N/\mathrm{d}t$ is expressed from the cosine law by

$$\cos I = \cos i\cos J - \sin i\sin J\cos\Omega \tag{21}$$

Next, by differentiating Eq. (21),

$$\frac{\mathrm{d}\Omega}{\mathrm{d}t} = \left(\cos J + \frac{\cos i}{\sin i}\sin J\cos\Omega\right)\frac{\mathrm{d}N}{\mathrm{d}t} \tag{22}$$

is obtained.

From the definition of ξ and η by Eq. (14),

$$\frac{\mathrm{d}\xi}{\mathrm{d}t} = \frac{\mathrm{d}e}{\mathrm{d}t}\cos\omega - e\sin\omega\frac{\mathrm{d}\omega}{\mathrm{d}t} = -\eta\frac{\mathrm{d}\omega}{\mathrm{d}t} \tag{23}$$

$$\frac{\mathrm{d}\eta}{\mathrm{d}t} = \frac{\mathrm{d}e}{\mathrm{d}t}\sin\omega + e\cos\omega\frac{\mathrm{d}\omega}{\mathrm{d}t} = \xi\frac{\mathrm{d}\omega}{\mathrm{d}t} \tag{24}$$

are derived. From the sine law,

$$\frac{\sin J}{\sin(W-\omega)} = \frac{\sin I}{\sin\Omega} \tag{25}$$

is obtained, and by differentiating this equation,

$$\frac{\mathrm{d}\omega}{\mathrm{d}t} = \frac{\mathrm{d}W}{\mathrm{d}t} - \frac{\sin J\cos\Omega}{\cos(W-\omega)\sin I}\frac{\mathrm{d}\Omega}{\mathrm{d}t} \tag{26}$$

is derived. From the cosine law,

$$\cos(W-\omega) = \cos\Omega\cos N + \sin\Omega\sin N\cos J \tag{27}$$

$\sin N$ is obtained by Eq. (19), and $\sin I$ and $\cos N$ are calculated by

$$\sin I = \sqrt{1-\cos^2 I} \tag{28}$$

$$\cos N = \frac{\cos i - \cos J\cos I}{\sin J\sin I} \tag{29}$$

The variation rates of the mean orbital elements just obtained are integrated numerically by the fourth-order Runge–Kutta method with a fixed step size of 1 day. The polar orbital plane has the freedom of 1 around the rotational axis of the asteroid. From the intrinsic constraints to each mission, the desirable orbital plane may be defined differently. In this study, however, $i = I = N = \Omega = 90$ deg were selected for the nominal orbital plane. The reasons for this selection are as follows.

1) This nominal orbital plane can be realized for any value of J.

2) If the orbit normal of this polar orbit nearly points to the sun and/or the Earth during the planned mission phase of several months, this selection might be advantageous to the maintenance of power and the communications with the Earth.

Results of Simulations

In this section, the four points a, b, c, and d in Fig. 2 are used for the simulation. The following conditions are used commonly for these four points:

$$R = 2\,\mathrm{AU} \Rightarrow \dot{\theta} = 0.35\,\mathrm{deg/day} \qquad B = 30\,\mathrm{kg/m^2}$$

The approximated variation rates of the mean orbital elements are given for convenience at the study of the simulated results as

$$\frac{\mathrm{d}\xi}{\mathrm{d}t} \fallingdotseq C_p \Delta i \cos\theta + \frac{1}{2} C_s \eta \tag{30}$$

$$\frac{\mathrm{d}\eta}{\mathrm{d}t} \fallingdotseq -C_p \sin\theta - \frac{1}{2} C_s \xi \tag{31}$$

$$\frac{\mathrm{d}i}{\mathrm{d}t} \fallingdotseq -C_p \xi \cos\theta + C_s \sin J (\Delta i \cos J - \Delta\Omega \sin J) \tag{32}$$

$$\frac{\mathrm{d}\Omega}{\mathrm{d}t} \fallingdotseq -C_p \eta \cos\theta + C_s \cos J (\Delta i \cos J - \Delta\Omega \sin J) \tag{33}$$

Elements with Δ indicate the deviation from 90 deg.

Point a in Fig. 2

Here $\alpha = 20\,\mathrm{km}$ and $a = 200\,\mathrm{km}$ ($a/\alpha = 10$). The characteristics of this orbit are shown in Table 2. The e_{limit} ($= 0.1$ in this study) is the keeping boundary for the eccentricity. Effects of the radiation pressure are larger than those of the oblateness to some extent in this orbit. Equations (30–33) show that the change of η is maximum because only the first term of $\mathrm{d}\eta/\mathrm{d}t$ does not have small quantities. The element that has the secondary large variation is Ω, because the first term of Eq. (33) has η.

Figure 5 shows the simulation results for $J = 0$ deg and $\theta_0 = 0$ deg. The direction of the change of η depends on the sign of $\sin\theta$ [see Eq. (31)]. Effects of J are very small. As Fig. 5 indicates, by selecting an adequately positive η in this case as the starting value, Ω can be returned to the initial point. This orbit can be kept by maneuvers with the interval of about 100 days.

Point b in Fig. 2

Here $\alpha = 20\,\mathrm{km}$ and $a = 100\,\mathrm{km}$ ($a/\alpha = 5$). The characteristics of this orbit are shown in Table 3. Effects of the oblateness are about 10 times of those of the radiation pressure in this orbit.

Table 2 Characteristics of orbit: α = 20 km and a = 200 km

Items	Symbols	Values
Acceleration by radiation pressure	F_R	5.708×10^{-8} m/s^2
Mean motion	n	1.308×10^{-5} rad/s $= 1.130$ rad/day
Orbital period	T	5.56 days
Characteristic angular velocity due to radiation pressure	C_p	0.002828 rad/day
Characteristic angular velocity due to oblateness	C_s	0.001695 rad/day
$C_p/(C_s\, e_{\mathrm{limit}})$		16.7 ($e_{\mathrm{limit}} = 0.1$)

Table 3 Characteristics of orbit: α = 20 km and a = 100 km

Items	Symbols	Values
Acceleration by radiation pressure	F_R	5.708×10^{-8} m/s^2
Mean motion	n	3.701×10^{-5} rad/s $= 3.197$ rad/day
Orbital period	T	1.97 days
Characteristic angular velocity due to radiation pressure	C_p	0.001999 rad/day
Characteristic angular velocity due to oblateness	C_s	0.01919 rad/day
$C_p/(C_s\, e_{\mathrm{limit}})$		1.04 ($e_{\mathrm{limit}} = 0.1$)

Table 4 Characteristics of orbit: α = 50 km and a = 200 km

Items	Symbols	Values
Acceleration by radiation pressure	F_R	5.708×10^{-8} m/s^2
Mean motion	n	5.172×10^{-5} rad/s $= 4.468$ rad/day
Orbital period	T	1.406 days
Characteristic angular velocity due to radiation pressure	C_p	0.0007152 rad/day
Characteristic angular velocity due to oblateness	C_s	0.04189 rad/day
$C_p/(C_s\, e_{\mathrm{limit}})$		0.17 ($e_{\mathrm{limit}} = 0.1$)

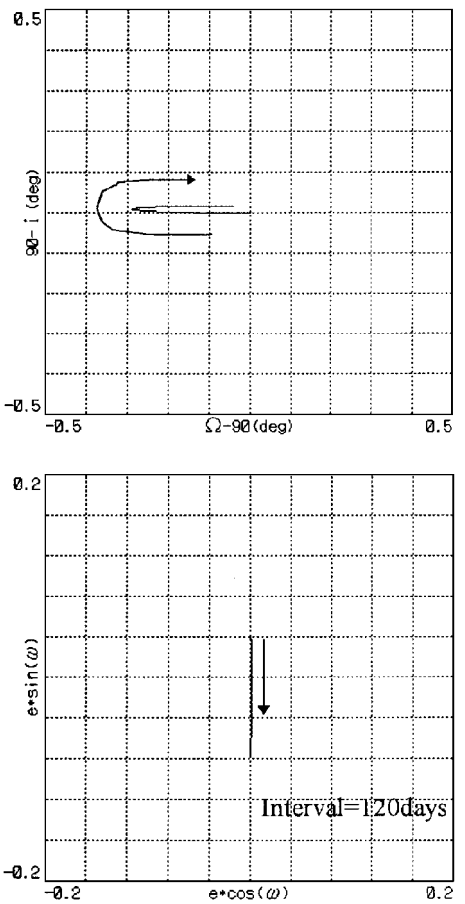

Fig. 5 Changes of e vector and orbital plane: α = 20 km, a = 200 km, J = 0 deg, θ_0 = 0 deg.

Figure 6 shows the simulation results for $J = 90$ deg and $\theta_0 = 0$ deg. This orbit also can be kept by maneuvers with the interval of about 100 days.

The change of ξ increased compared with Fig 5. This increased change of ξ can be explained by the second term of Eq. (30). The change of i also increased due to the increased ξ in the first term and the increased C_s in the second term of Eq. (32). Though Ω can be returned at the time of the next maintenance maneuver, the deviation of i cannot be removed. Maneuvers for i might be necessary if a mission life of several years is required.

Point c in Fig. 2

Here $\alpha = 50\,\mathrm{km}$ and $a = 200\,\mathrm{km}$ ($a/\alpha = 4$). Figure 7 shows the 1000-day simulation results of this orbit for $J = 0$ deg and $\theta_0 = 90$ deg. This orbit needs no maneuvers for maintenance with e_{limit} of 0.1.

The characteristics of this orbit are shown in Table 4. Effects of the oblateness are about 60 times of those of the radiation pressure in this orbit.

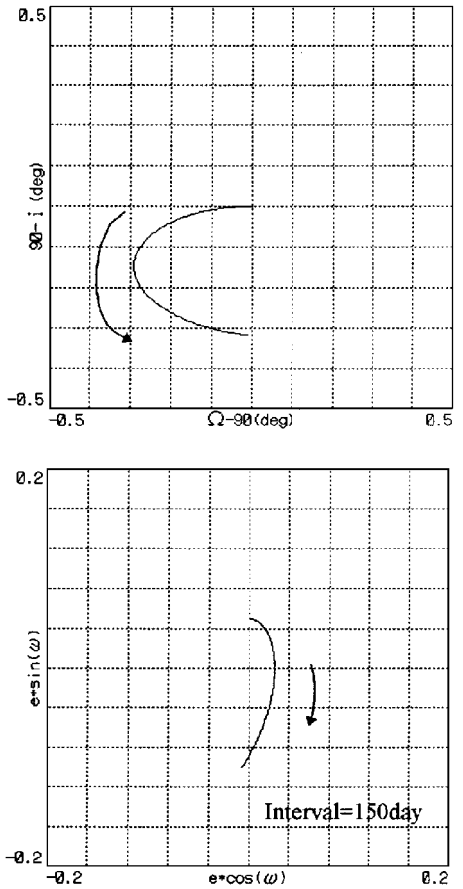

Fig. 6 Changes of e vector and orbital plane: α = 20 km, a = 100 km, J = 90 deg, θ_0 = 0 deg.

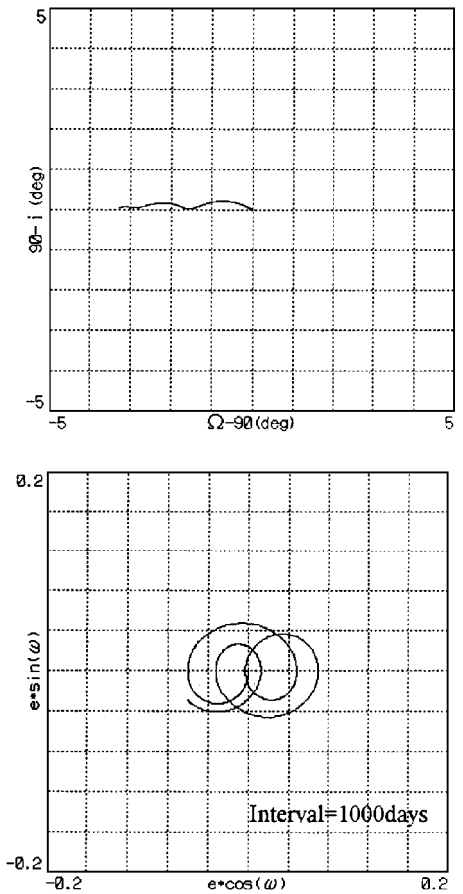

Fig. 7 Changes of e vector and orbital plane: α = 50 km, a = 200 km, J = 0 deg, θ_0 = 90 deg.

Table 5 Characteristics of orbit: α = 100 km and a = 300 km

Items	Symbols	Values
Acceleration by radiation pressure	F_R	5.708×10^{-8} m/s^2
Mean motion	n	7.962×10^{-5} rad/s $= 6.880$ rad/day
Orbital period	T	0.913 days
Characteristic angular velocity due to radiation pressure	C_p	0.0003097 rad/day
Characteristic angular velocity due to oblateness	C_s	0.1147 rad/day
$C_p/(C_s\, e_{\text{limit}})$		0.027 ($e_{\text{limit}} = 0.1$)

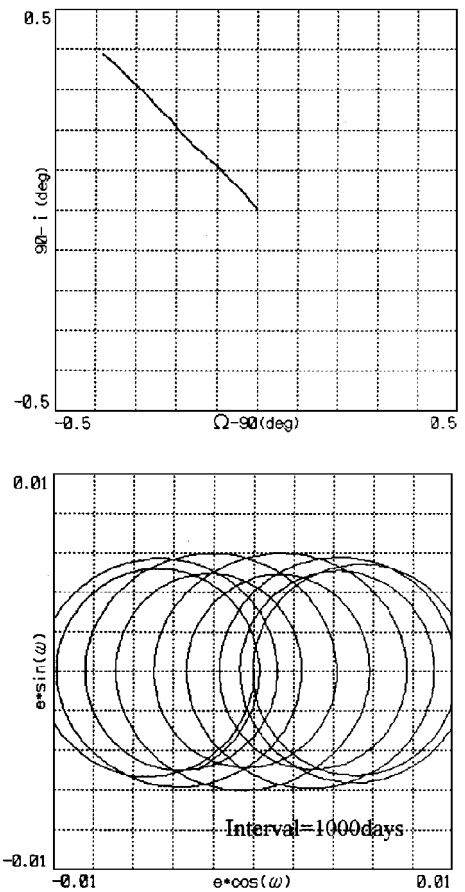

Fig. 8 Changes of e vector and orbital plane: α = 100 km, a = 300 km, J = 45 deg, θ_0 = 90 deg.

Because the order of Δi and (ξ, η) are 0.01 rad and 0.1, respectively, the second terms of Eqs. (30) and (31) are dominant. Then, the motion of the eccentricity vector becomes like a harmonic oscillation. The angular velocity for the motion is $C_s/2$. The change direction of the orbital plane depends on J from the second terms of Eqs. (32) and (33) (see Figs. 7 and 8).

Point d in Fig. 2

Here $\alpha = 100$ km and $a = 300$ km ($a/\alpha = 3$). Figure 8 shows the 1000-day simulation results of this orbit for $J = 45$ deg and $\theta_0 = 90$ deg. This orbit also needs no maneuvers for maintenance.

The characteristics of this orbit are shown in Table 5. Effects of the oblateness are about 370 times of those of the radiation pressure in this orbit.

Conclusions

From the study for the feasible regions of the frozen orbits, the following results were found.

1) The frozen orbits in the orbital plane are feasible for asteroids whose radii are about 40–50 km.

2) The solar plane-of-sky frozen orbits are feasible for asteroids whose radii are smaller than about 3 km.

3) The frozen orbits in the orbital plane have large altitudes. Therefore, they are not adequate for the observation with high resolution.

If the altitude of the frozen orbit in the orbital plane is reduced, effects of oblateness become large and the necessary condition for the frozen orbit is not satisfied. Though the altitude-reduced frozen orbit in the orbital plane can be maintained by maneuvers, a velocity increment of about 100 m/s for 1-year maintenance is required for the orbit whose semimajor axis is about three times of the asteroid's radius.

Next, polar orbits were studied because they have the following advantages.

1) The polar orbital plane is not affected by the oblateness of the asteroid.

2) The solar radiation pressure does not change orbital planes if the eccentricity is controlled to be zero. The required ΔV for this control is very small.

3) The rotational motion of the asteroid can be utilized for global mapping of the asteroid.

Variations of the eccentricity vector and the orbital plane of the near circular polar orbit due to the radiation pressure and the oblateness were studied by numerical integrations of the mean orbital elements. When $C_p/(C_s e_{\text{limit}})$ is larger than about 1, eccentricity control is required about every 100 days in the case of $e_{\text{limit}} = 0.1$. When $C_p/(C_s e_{\text{limit}})$ is smaller than about 1, the polar orbit does not need the eccentricity control (see Tables 2–5).

From these studies, a guideline for the design of orbits around asteroids whose radii are smaller than 100 km can be made as follows.

1) The solar plane-of-sky frozen orbit is the first candidate for asteroids whose radii are smaller than about 3 km.

2) The polar orbit is the first candidate for the other asteroids.

Asteroids whose radii are smaller than about 3 km have the possibility that the rotational motion is not simple around the principal axis. This motion is, however, not a problem for the selection of the solar plane-of-sky frozen orbit. For larger asteroids, simple rotation can be expected. Therefore, the polar orbit can be selected.

Because this is a study using the mean orbital elements, detailed studies by the osculating orbital elements are necessary hereafter.

References

[1]Farquhar, R. W., "Introduction: The Near-Earth Asteroid Rendezvous (NEAR) Mission," *Journal of the Astronautical Sciences*, Vol. 43, No. 4, 1995, pp. 349–351.

[2]Matsuo, H., Kawaguchi, J., Fujiwara, A., and Uesugi, T., "The Near Earth Asteroid Sample and Return Mission, MUSES-C," *Proceedings of the 20th International Symposium on Space Technology and Science*, 1996, pp. 1123–1128.

[3]Chobotov, V. A. (ed.), *Orbital Mechanics,* AIAA Education Series, AIAA, Washington, DC, 1991, pp. 310–311.

[4]Scheeres, D. J., "Satellite Dynamics About Asteroids," American Astronomical Society, AAS 94-112, Feb. 1994.

[5]Scheeres, D. J., "Dynamics About Uniformly Rotating Tri-Axial Ellipsoids. Application to Asteroids," *Icarus International Journal of the Solar System*, Vol. 110, 1994, pp. 225–238.

[6]Hirota, M., "Long Periodic Solutions of Geostationary Orbital Plane and Eccentricity Vector by Means of the General Perturbations Method," National Space Development Agency, TR-16, Tsukuba-shi, Japan, 1983.

[7]Watanabe, J., "Rotation of Comets and Asteroids in Families," *Seventy-Five Years of Hirayama Asteroid Families: The Role of Collisions in the Solar System History*, Astronomical Society of the Pacific Conf. Series, Vol. 63, 1994, pp. 150–153.

F. H. Lutze Jr.
Associate Editor